A resolved mantle anomaly as the cause of the Australian-Antarctic Discordance

M.H. Ritzwoller[††], N.M. Shapiro, and G.M. Leahy[†]

Center for Imaging the Earth's Interior

Department of Physics

University of Colorado

Campus Box 390, Boulder, CO 80309, USA

† Now at: Geology and Geophysics Department, Yale University, New Haven, CT 06520-8109 USA

†† To whom correspondence should be directed: ritzwoller@ciei.colorado.edu

Submitted to *J. Geophys. Res.*: March 27, 2003.
Revised: September 12, 2003. In press: September, 2003.

Abstract

We present evidence for the existence of an Australian-Antarctic Mantle Anomaly (AAMA) that trends northwest-southeast (NW-SE) through the Australian-Antarctic Discordance (AAD) on the Southeast Indian Ridge (SEIR), is confined to the upper 120 km of the mantle beneath the AAD, and dips shallowly to the west so that it extends to a depth of about 150 km west of the AAD. Average temperatures within the AAMA are depressed about 100°C relative to surrounding lithosphere and suggest very rapid cooling of newly formed lithosphere at the AAD to an effective thermal age between 20 - 30 Ma. A convective down-welling beneath the AAD is not consistent with the confinement of the AAMA in the uppermost mantle. In substantial agreement with the model of Gurnis et al. (1998), we argue that the AAMA is the suspended remnant of a slab that subducted at the Gondwanaland-Pacific convergent margin more than 100 Ma ago, foundered in the deeper mantle, and then ascended into the shallow mantle within the past 30 Ma cutting any ties to deeper roots. The stability of the AAMA and its poor correlation with residual topography and gravity imply that it is approximately neutrally buoyant. The thermally induced density anomaly can be balanced by bulk iron depletion of less than 0.8%, consistent with the warmer conditions of formation for the Pacific than Indian lithosphere. We hypothesize that the low temperatures in the AAMA inhibit crustal formation and the AAD depth anomaly is formed at the intersection of the SEIR and the AAMA. The northward migration of the SEIR overriding the cold NW-SE trending AAMA, therefore, presents a simple kinematic explanation for both the V-shaped residual depth anomaly in the southeast Indian Ocean and the western migration of the AAD along the SEIR. Neither explanation requires the Pacific asthenospheric mantle to push westward and displace Indian asthenosphere. The AAMA may also act as a barrier to large-scale flows in the shallow asthenosphere and may, therefore, define a boundary for mantle convection and between the Indian and Pacific isotopic provinces. The westward dip of the AAMA would also favor along-axis flow from the Indian Ocean asthenosphere to the AAD that may contribute to the penetration of Indian Ocean MORBs into the AAD.

1. Introduction

The Australian-Antarctic Discordance (AAD) (e.g., Weissel and Hayes, 1971, 1974) is a portion of the Southeast Indian Ridge (SEIR) between 120°E and 128°E longitude characterized by a chaotic ridge pattern and a negative depth anomaly (Figure 1). The AAD is the deepest segment of the world's mid-ocean ridge system and marks a geochemical boundary between Pacific and Indian type mid-oceanic ridge basalts (e.g., Klein *et al.*, 1988). Analysis of local bathymetry as well as magnetic and gravity anomalies shows that the AAD depth anomaly has existed for at least 25 Ma and during the last 20 Ma has migrated westward at a rate of approximately 15 mm/yr (e.g., Marks et al., 1999). The geochemical boundary has also migrated westward but apparently at a somewhat faster rate (e.g., Pyle et al., 1995). The origin of the depth anomaly at the AAD is generally attributed to colder than normal mantle temperatures below this segment of the SEIR, consistent with the major element systematics for basalts from the AAD (Klein and Langmuir, 1987). This thermal anomaly may inhibit magma production along the ridge and thin the oceanic crust (Tolstoy et al., 1995). Several hypotheses concerning the cause of a cold mantle anomaly below the AAD have been proposed, including the existence of a stable cold-spot (Hayes, 1976), convective down-welling (e.g., Hayes, 1988; Klein et al., 1988), reduced up-welling (Kuo, 1993; Kuo et al., 1995), passive along-axis flow in response to colder temperatures along the ridge segment (e.g., Forsyth *et al.*, 1987; West *et al.*, 1997), and the presence of a stagnated slab that subducted beneath the Gondwanaland-Pacific margin and was subsequently drawn by the southeast Indian Ridge beneath the AAD (Gurnis *et al.*, 1998). Gurnis et al. have recently elaborated their model by presenting evidence that the AAD results specifically from the effect of an old mantle wedge (Gurnis and Müller, 2003).

The AAD has been the subject of several previous seismic studies. Both surface wave dispersion (e.g. Forsyth *et al.*, 1987; Kuo *et al.*, 1996) and SS-S travel time residuals (Kuo, 1993) have shown that the upper mantle beneath the AAD is characterized by faster than normal seismic velocities, which indicates that the lithosphere beneath the AAD thickens anomalously quickly and the asthenosphere is cooler than average. Global models, too, display

fast uppermost mantle beneath the southeast Indian Ocean at large-scales (e.g., Zhang and Tanimoto, 1993; Masters et al., 2000). Gurnis and Müller (2003) present a detailed comparison between three recent global mantle models in this region.

The purpose of the present study is to produce more detailed 3-D seismic images of the upper mantle beneath the southeast Indian Ocean and surroundings to illuminate the nature and cause of the AAD. We base these images on the recent work of Ritzwoller *et al.* (2001), but have expanded the data-set of surface-wave group speed dispersion measurements and have improved methods of surface-wave inversion (Ritzwoller et al., 2002; Shapiro and Ritzwoller, 2002a, 2003). The result is a higher resolution and more reliable shear-velocity model of the upper mantle beneath the southeast Indian Ocean.

We present evidence for an Australian-Antarctic mantle anomaly (AAMA) that is confined to the top 120 km of the uppermost mantle beneath the AAD and extends in the northwest-southeast (NW-SE) direction through the AAD. We argue that, by affecting crustal formation, the AAMA is the principal cause of the AAD topographic anomaly along the SEIR, and also plays an important role in other observables such as the westward migration of the AAD along the SEIR, the V-shaped residual depth anomaly in the southeast Indian Ocean, and the location of a geochemical province boundary. Its presence and orientation provide new and simple kinematical explanations for a number of the characteristics that define the AAD and its surroundings.

2. Data and Surface Wave Tomography

The 3-D seismic model is based on broad-band surface wave group and phase velocity measurements. The group velocities were measured using the method described by Ritzwoller and Levshin (1998), a frequency-time method that involves analyst interaction to choose the frequency band of measurement and to guide the extraction of the fundamental mode from noise, scattered and multipathed signals, overtones, and fundamental modes of different wave types. We use group velocity measurements from 16 sec to 200 sec period for Rayleigh waves and from 16 sec to 150 sec period for Love waves. We only use group velocity measurements

from earthquakes shallower than 50 km to reduce the size of the source group time shifts, which we do not attempt to correct (Levshin *et al.*, 1999). The phase velocity measurements were performed at Harvard University and Utrecht University separately and we merged these data-sets. The phase velocity measurements extend from 40 sec to 150 sec for both Rayleigh and Love waves. These data-sets are described by Ekström et al. (1997) and Trampert and Woodhouse (1995). All measurements are subjected to the quality control procedures described by Ritzwoller and Levshin (1998). We devoted particular efforts to analyzing earthquakes located on the SEIR observed at SKIPPY stations in Australia. The resulting average path density for the region surrounding the AAD is shown in Figure 2a.

Although we produce dispersion maps on a $2^\circ \times 2^\circ$ grid globally (e.g., Shapiro and Ritzwoller, 2002a), maps of the region of study are produced on a $1^\circ \times 1^\circ$ sub-grid. The construction of the group and phase velocity maps is based on diffraction tomography (Ritzwoller et al., 2002), which is an update of the tomographic method of Barmin et al. (2001). Diffraction tomography uses a simplified version of the scattering sensitivity kernels that emerge from the Born or Rytov approximations, and accounts for path-length dependent sensitivity, wave-front healing and associated diffraction effects, and provides a more accurate assessment of spatially variable resolution than traditional tomographic methods based on ray theory. The resolution method is described by Barmin et al. (2001). We produce a resolution surface at every node on the globe, fit a 2-D Gaussian surface in the neighborhood of each node, and define resolution as twice the standard deviation of the surface Gaussian. Lateral resolution estimates averaged over the region of study are presented in Figure 2b. Resolution degrades with period, but below 100 sec, where waves are most sensitive to the uppermost mantle, Rayleigh wave resolution ranges from 400 to 700 km for group velocities and 800 to 900 km for phase velocities. These results will be used in a resolution test in section 4.1.

Figures 2c and 2d show the Rayleigh-wave group velocity maps at periods of 45 sec and 70 sec, respectively. Both maps display a high-velocity anomaly that extends in the NW-SE direction through the AAD. These maps are characteristic of the 30-100 sec range for the Rayleigh wave maps; all of which display a high velocity anomaly trending NW-SE through the AAD.

3. 3-D Shear-Velocity Model

The shear-velocity model is constructed using a Monte-Carlo method, which is described in detail by Shapiro and Ritzwoller (2002a). The inversion is performed at each node on a $1^\circ \times 1^\circ$ grid across the region of study, and produces an ensemble of acceptable models down to a depth of 400 km. The model is constrained by a variety of *a priori* information, including the initial crustal model CRUST2.0 (G. Laske, personal communication). Shapiro and Ritzwoller (2002a) fully describe the set of constraints. The isotropic part of the model in the mantle is parameterized with B-splines.

Figure 3 displays an example of the inversion at the starred point in Figure 1 near the center of the AAD. Measurements taken from the dispersion maps are shown in Figure 3a. The error bars are twice the rms-misfit between the dispersion measurements and the predictions from the dispersion maps averaged over the southern hemisphere, as described by Ritzwoller et al. (2001). Due to the absence of reliable uncertainty information about the dispersion maps at each point, Shapiro and Ritzwoller (2002a) use this rms-misfit to weight the dispersion measurements during inversion. The rms-misfit between the dispersion measurements and the predictions from the dispersion maps, therefore, is used as a standard deviation, σ, and the error bars shown in Figure 3 can be thought of as 2σ uncertainties. We find that the uncertainties, defined in this way, fairly accurately reflect at least our relative confidence in the values obtained from the dispersion maps.

Figure 3b presents the ensemble of models that fits the observations at this point acceptably. The range of dispersion curves predicted from this ensemble is plotted over the observations in Figure 3a. The model is radially anisotropic ($V_{sh} \neq V_{sv}$) from the Moho to a variable depth that averages about 200 km. We will not discuss the anisotropic properties of the model further, but will concentrate only on the isotropic component of shear velocity ($V_s = (V_{sh} + V_{sv})/2$) at all depths. We note, however, that in the neighborhood of the AAD the general features found in V_s, V_{sh}, and V_{sv} are very similar, only the absolute values differ. The ensemble of acceptable models widens appreciably below about 200 - 250 km, on average, and the model is, therefore, most reliable in the top $\sim$200 km. Figures 3c - 3e demonstrate the

importance of simultaneously inverting the group and phase speeds. In particular, the vertical resolution of the model is substantially improved in the uppermost mantle by introducing the group speeds, which extend to shorter periods than the phase speeds. Introduction of phase speeds improves resolution below ~150 km. We summarize the acceptable models with a single model taken at the middle of the corridor of acceptable models. We refer to this as the ensemble median model or simply as the V_s model (e.g., the bold line in Figure 4).

Because of the cooling of the oceanic crust and lithosphere after formation, the predominant feature in seismic models of the oceanic upper mantle is the formation of a lithospheric lid and the diminishment of the strength of the low-velocity zone as the lithosphere ages (e.g., Shapiro and Ritzwoller, 2003). This age-dependent trend is clear in our model of the Southeast Indian Ocean, as the lithospheric age averages in Figure 4 illustrate. These age-dependent (or age-averaged) models are computed by segregating the southeast Indian Ocean into age provinces (Müller et al., 1997) and averaging the models at each depth over each province. Anomalous topographic features such as continental shelfs, the Kerguelen Plateau, the Diamantina Fracture Zone, and the AAD region were removed during the averaging of the seismic model.

Misfit statistics for various models to the dispersion measurements at the AAD (Figure 4) are presented in Table 1. Misfit is normalized by the uncertainties, σ, shown in Figure 3a, defined as follows

$$\chi - \text{misfit} = \left(\frac{1}{N} \sum_{i=1}^{N} \left(\frac{d_i - \hat{d}_i}{\sigma_i} \right)^2 \right)^{1/2} \quad (1)$$

where N is the number of dispersion measurements, d is the observed group or phase speed, and $\hat{d}$ is the group or phase speed predicted from the specified model. Of the age-dependent models, the 20 Ma model fits the dispersion data near the AAD, nearly indistinguishably from the ensemble median model.

Figure 5 shows several horizontal and vertical slices of the V_s model beneath the southeast Indian Ocean. We remove the age-dependent trend (examples in Figure 4) from these images to emphasize the features that are independent of age. The uppermost mantle beneath the AAD displays a high-velocity anomaly, relative to the age-dependent trend, to a depth of about 120

km. This Australian-Antarctic Mantle Anomaly (AAMA) extends in the northwest-southeast (NW-SE) direction through the AAD and has a gentle westward dip of about 15° relative to the horizontal along the SEIR. The Monte-Carlo inversion allows us to identify the features that appear in every member of the ensemble of acceptable models. We call these features "persistent" and, as Figure 5c shows, the AAMA is only deemed persistent to a depth of about 120 km beneath the AAD and somewhat deeper ($\sim$ 150 km) to the west of the AAD along the SEIR. At greater depths, this high velocity anomaly is absent and a low velocity anomaly eventually emerges south of the AAD as shown in Figure 5b.

The general features of the AAMA (orientation, horizontal and depth extent, amplitude of the velocity anomaly) are quite robust relative to ad-hoc choices in damping and to details of the tomographic and inversion procedures. We have, for example, also constructed models in which the surface wave tomography is based on ray-theory with ad-hoc Gaussian smoothing rather than diffraction tomography. In addition, we constructed models in which the seismic parameterization was replaced with an intrinsically thermal parameterization (defined in section 4.3). In each case we found changes in detail, but the general features of the estimated AAMA model remain substantially unchanged.

Aspects of the AAMA have been observed previously from regional surface wave studies of the southeast Indian Ocean. Using Rayleigh wave phase speeds observed at Australian stations from several events along the SEIR, Forsyth et al. (1987) showed that beneath young sea floor the primary anomalous feature is a lithospheric lid extending at least to 40 km depth. They also showed that the low velocity zone was less pronounced than in the Pacific, beneath crust both less than and greater than 10 Ma. These observations are in substantial agreement with the model shown in Figure 5. In a similar study based on group speeds, Kuo et al. (1996) argued for an elongated velocity anomaly in the uppermost mantle centered about 400 km west of the AAD and stretching northward about 1000 km. The extent of this anomaly is similar to the AAMA, but the orientation is different. The use of a larger set of regional data, in particular measurements obtained at SKIPPY stations in Australia, has allowed us to resolve the orientation of this feature, trending NW-SE through the AAD. The location of the anomaly observed on the dispersion maps is actually period dependent, and it can be

misleading to infer the orientation of the mantle feature from narrow band dispersion maps alone. In particular, because the AAMA dips to the west beneath the SEIR, the high speed AAD anomaly in the dispersion maps shifts to the west as period increases. This is probably why the global model of Zhang and Tanimoto (1993), cited by Kuo et al. (1996), displays the high speed mantle anomaly to the west of the AAD – this global model is based only on very long period dispersion data. The AAMA shown in Figure 5 is able to fit both the short period group speed data that orient the anomaly through the AAD and the longer period dispersion measurements that require the AAMA to dip to the west beneath the SEIR.

4. The Nature and Extent of the AAMA

Before considering the cause of the AAMA, we will address several preliminary issues concerning its nature and extent. The first issue relates to vertical resolution. Although the AAMA is observed to be a "persistent" anomaly only to a depth of about 120 km below the AAD, we consider the possibility that the anomaly extends to significantly greater depths but the surface waves simply do not resolve it. The second issue concerns how the seismic (and presumably thermal) structure beneath the AAD compares to normal oceanic lithosphere across the southeast Indian Ocean, particularly as a function of lithospheric age. This issue relates to how the lithosphere forms and evolves beneath and adjacent to the AAD. Finally, the third issue concerns whether the AAMA is entirely a temperature anomaly. We consider evidence that the AAMA is also compositionally distinct from the surrounding mantle.

4.1 Depth extent of the AAMA

The range of models that emerge from the Monte-Carlo inversion reflects uncertainties associated with the limited and variable depth sensitivity of the surface waves. It does not, however, account for the diminishment of lateral resolution with depth caused by the reduction of resolution at long periods, as seen in Figure 2b. Therefore, the deeper features of the model at the length scales of the AAMA (< 1000 km) are significantly less robust than the shallower features. It remains to be determined if the AAMA could, in fact, extend to depths greater

than ∼120 km.

To address this issue we created a 2-D synthetic model with a fast slab-like anomaly of Gaussian cross-section in the upper mantle. The characteristics of this synthetic anomaly (amplitude, width, and dip angle) reflect the observed properties of the AAMA, except the feature extends down to the transition zone (Figure 6a). The slab anomaly plotted in Figure 6a is added to the 1 Ma average model for the southeast Indian Ocean (Figure 4). The dispersion curves for this synthetic model are inverted using the same Monte-Carlo method applied to the real data. The results of the inversion, presented Figure 6b, show that the slab-like feature is well recovered all the way to the transition zone. To account for the effects of the variation of lateral resolution with period and wave-type, a second inversion was performed in which the synthetic dispersion curves were smoothed horizontally to mimic the estimated resolution shown in Figure 2b. The results of this second test are shown in Figure 6c. Although the recovered anomaly widens with depth due to the degradation in resolution at long periods, a fast anomaly is apparent to depths well below the 120 km depth that we argue is the greatest depth to which the AAMA extends. Note that the results presented here are for V_{sv} for which lateral resolution is better than either V_{sh} or V_s. Similar results are seen in V_{sh} or V_s but the broadening with depth is greater in these velocities.

These resolution tests show that the continuation of the AAMA to depths greater than about 120 km is not likely unless the deeper reaches of the anomaly have significantly smaller amplitudes than the shallower parts. We are confident, therefore, that the AAMA is largely confined to the top 120 km of the upper mantle beneath the AAD, although it dips somewhat deeper to the west. It may, however, be underlain in the transition zone and uppermost lower mantle by a high velocity anomaly, as revealed by recent global mantle images (e.g., Masters et al., 2000). We discuss the possibility of a genetic relationship between these anomalies in a later section. As in any inversion, the AAMA may be sharper and its amplitude may be larger than our tomographic images reflect.

4.2 Comparison of mantle beneath the AAD with "normal" oceanic mantle

We use two different methods to assess how mantle structure beneath the AAD compares with other non-anomalous oceanic lithosphere across the southeast Indian Ocean.

4.2.1 Similarity analysis The first method is a direct comparison between the model at the AAD with the model at other locations. We define the "similarity" S between a model at two points in space, $v(z)$ and $v_{\mathrm{ref}}(z)$, as the depth integrated weighted one-norm difference between the two 1-D profiles:

$$S = 1 - N^{-1} \int \sigma^{-1}(z) \left| v(z) - v_{\mathrm{ref}}(z) \right| dz, \tag{2}$$

where $N = \int dz$,and $\sigma(z)$ is the uncertainty in the reference model v_{ref} at depth z defined by the half-width of the ensemble of acceptable models. The limits on the integrals are 20 km and 130 km, respectively. S lies between 0 and 1 for similar vertical profiles; in particular, $S = 1$ for identical profiles. If $S < 0$ we consider the two 1-D profiles to be dissimilar. Similarity is reminiscent of two-point correlation, but two perfectly correlated models will be dissimilar if they are offset by an appreciable constant velocity.

An example is shown in Figure 7 in which the reference profile is taken at the starred location within the AAD shown in Figure 1. The grey-shaded regions are the parts of the southeast Indian Ocean mantle that are similar to the mantle beneath the AAD. On average, the upper mantle beneath the AAD is similar to the parts of the southeast Indian Ocean outside the AAD region with lithospheric ages ranging from about 15 - 30 Ma.

4.2.2 Thermal parameterization of mantle structure The second method to compare mantle structure beneath the AAD with lithosphere underlying the rest of the southeast Indian Ocean is based on the thermal model parameterization described by Shapiro and Ritzwoller (2003). In this method, the seismic parameterization used to define the model shown in Figure 5 is replaced by an intrinsically thermal model (Figure 8a) in which a conductive layer is underlain by a mantle adiabat. Although this thermal model is most appropriate for non-anomalous oceanic lithosphere, we believe that results in the neighborhood of the AAD are meaningful even though the AAD is an anomalous ridge segment. The thermal parameterization is used here exclusively as a consistency check on the results obtained from

the similarity analysis applied to the model derived using the seismic parameterization. All figures here except Figure 8 originate from the seismic parameterization and all inferences can derive from the seismic parameterization alone. Nevertheless, as we show, the results with the thermal parameterization agree with those from the seismic parameterization and confirm the results of the similarity analysis.

In the thermal model, temperatures within the conductive layer are given by an error function whose characteristics are determined by its apparent thermal age, τ_c, and within the convective mantle by the potential temperature, T_p. The apparent thermal age summarizes the structure of the lithosphere and potential temperature represents asthenospheric structure. The coefficient of thermal diffusivity, κ, and the adiabatic gradient, D, are assumed to be known within the mantle. Therefore, the mantle temperature profile is determined by only two unknowns, τ_c and T_p. The Monte-Carlo inversion proceeds as with the seismic parameterization, except that models are randomly generated in temperature space and converted to isotropic shear velocity using a mineralogical model of average oceanic composition (Dick et al., 1984), laboratory-measured thermo-elastic properties of individual minerals, the Voigt-Reuss-Hill averaging scheme, and an anelastic model. This conversion is based on the method of Goes et al. (2000) and is described in detail by Shapiro and Ritzwoller (2003). After converting each candidate thermal model to isotropic shear velocity, radial anisotropy with randomly chosen strength and depth extent is introduced, so each candidate shear velocity model is radially anisotropic between the Moho and about 200 km depth, as with the seismic parameterization discussed above. Candidate models are promoted into the acceptable category if they satisfactorily fit the dispersion information. We report here ensemble averages for τ_c and T_p.

The estimated apparent thermal age across the southeast Indian Ocean is shown in Figure 8b. The thermal age of the AAD is seen to be elevated relative to the rest of the SEIR. Figure 8c demonstrates that the thermal age at the AAD is between 20 - 30 Ma greater than expected for newly formed lithosphere. This "excess thermal age" follows the strike of the AAMA NW-SE through the AAD. Figure 8d shows the potential temperature beneath the southeast Indian Ocean. Similar to Figure 5b, this demonstrates that asthenospheric temperatures on

the Antarctic Plate to the south of the AAD are elevated.

The conclusion from both the similarity analysis and the thermal parameterization (i.e., thermal age estimates) is that the seismic and temperature structures of the lithosphere beneath the AAD more nearly resemble 20 - 30 Ma lithosphere than the lithosphere beneath normal spreading ridges. This conclusion also agrees well with evidence provided by Forsyth et al. (1987) that phase speeds beneath young lithosphere where the residual depth anomaly is greater than 500 m are significantly elevated relative to Pacific sea floor of comparable age.

4.3 Is the AAMA a purely thermal anomaly?

Using the conversion between temperature and shear velocity discussed in section 4.2, we convert the 3-D model derived using the seismic parameterization into temperature and density. The resulting temperature anomalies along the SEIR are shown in Figure 9. The lowest temperature anomaly beneath the AAD is about 200°C at 60 km depth, but the spatial average of the temperature depression within the AAMA is about 100°C with respect a regional average. This average is similar to the mean temperature anomaly reported in previous studies, although individual earlier estimates varied substantially between studies (e.g., Forsyth et al., 1987; Klein and Langmuir, 1987; Hayes, 1988; Forsyth, 1992; Kuo, 1993; Shen and Forsyth, 1995; Sempere et al., 1997; West et al., 1997; Gurnis et al., 2000). The low temperatures beneath the AAD are qualitatively consistent with the AAD depth anomaly and suggest a rapid cooling of newly formed lithosphere to an effective thermal age of between 20 to 30 Ma. To be believed, the density anomalies that result from these low temperatures must be consistent with sea floor topography as well as the apparent long-term stability of the AAMA over at least the past 25 Ma.

Density anomalies are computed from the temperatures shown in Figure 9 using a coefficient of thermal expansion $\alpha = 3.0 \times 10^{-5}$ K^{-1}. These anomalies can be used to compute the relative bathymetry Δh along the SEIR assuming isostatic compensation in the mantle:

$$\Delta h = \frac{1}{\rho_m - \rho_w} \int_{z_0}^{z_c} (\rho(z) - \rho_{\mathrm{ref}}(z))\, dz \tag{3}$$

where z_c is the depth of compensation (chosen to be 130 km), z_0 is fixed at 20 km to avoid the crustal contribution, $\rho(z)$ is the density profile of the column in question, and ρ_m and ρ_w are average densities of the mantle and water, respectively. The reference mantle density, ρ_{ref}, is chosen to minimize the average difference between the predicted and observed topography along the SEIR. It is, therefore, only the variation in topography that is predicted by the seismic model. This prediction of topography derives exclusively from the mantle contribution down to a depth of 130 km; the crust is assumed to be laterally homogeneous and does not contribute to the relative topography.

The mantle contribution to bathymetry along 50°S predicted in this way from the 3-D shear velocity model fits the shape and the magnitude of the observed bathymetry rather well, as Figure 10 shows. It is tempting, therefore, to hypothesize that the AAMA is a purely thermal anomaly that is dense, intrinsically negatively buoyant, and isostatically compensated by topography on the sea floor beneath the SE Indian Ocean.

There are several problems with this hypothesis, however. First, if we would correct the observed bathymetry for crustal thickness variations along the SEIR, the topography would become strongly overpredicted. Tolstoy et al. (1995) present evidence that the crust within the AAD is about 3 km thinner than along the adjacent ridge segments. This would accommodate more than half of the observed topography anomaly. Therefore, either the temperature anomalies shown in Figure 9 are too large by about a factor of two or the AAMA beneath the AAD is supported by some other means. Given uncertainties in the V_s-to-temperature conversion, the temperature anomalies in Figure 9 may, in fact, be overestimated, but there are three other severe problems for the hypothesis. Second, the AAMA does not correlate with the V-shaped off-ridge residual depth anomalies beneath the southeast Indian Ocean as shown in Figure 11. Only at the AAD is the AAMA coincident with residual depth anomalies. It is, therefore, unlikely that the AAMA is compensated isostatically by sea floor topography in a general sense across the southeast Indian Ocean. Third, there is no pronounced geoid or long-wavelength gravity anomaly associated with the AAMA. Given the absence of topographic anomalies northwest of the AAD, if the AAMA is denser than surrounding mantle it should have a clear gravity signature. Finally, if it is the cause of the AAD, the AAMA must have

existed in the uppermost mantle at least as long as the AAD; i.e., for >25 Ma . If the AAMA is as dense as predicted under the assumption of the very cool temperatures shown in Figure 9 with average Indian Oceanic composition, it must be supported by some other means in order to be nearly neutrally buoyant.

One way to explain these observations is that the AAMA is not in isostatic equilibrium but is dynamically supported. Although this alternative cannot be ruled out, we see no direct evidence for low seismic velocities (hence, high temperatures) underlying the full extent of the AAMA, although high temperatures can be inferred beneath the AAMA on the Antarctic Plate south of the SEIR. It is possible, however, that the compensation is deeper than the ~200-250 km depth to which our 3-D model extends. But, the greater the depths of the supporting anomaly, the less likely it will be to produce the relatively sharp topographic features needed to compensate for the topography that the AAMA would impart isostatically to the sea floor.

A more plausible possibility is that the AAMA is not purely a thermal anomaly but is compositionally distinct from normal mantle beneath the southeast Indian Ocean. More specifically, the AAMA may be composed of mantle minerals that are more depleted in heavier elements than surrounding mantle. The density perturbations caused by the compositional and thermal anomalies approximately balance, but the effects on the seismic wave speeds are additive. As a result, the AAMA is seismically fast, but may be approximately neutrally buoyant. This will be discussed further in the next section.

5. The Cause and Implications of the AAMA

We have presented evidence for the existence of an Australian-Antarctic Mantle Anomaly (AAMA) that trends NW-SE through the Australian-Antarctic Discordance (AAD), is confined to the upper 120 km of the mantle beneath the AAD, and dips shallowly to the west so that it extends to a depth of about 150 km west of the AAD. We have also shown that lithospheric structure beneath the AAD resembles normal oceanic lithosphere with ages between 20 to 30 Ma. Finally, we have argued that in the absence of deeper dynamical support, the AAMA

must be approximately neutrally buoyant. Thus, the AAMA is not purely thermal in origin but is probably also compositionally distinct from surrounding mantle such that the thermally induced density anomalies are approximately balanced by depletion in heavy elements. How, then, has the AAMA formed and what are the implications for other observables?

5.1 The AAMA as a suspended slab remnant

It has been often proposed that the AAD is caused by convective down-welling in response to along-axis asthenospheric flow (e.g., Veevers, 1982; Vogt et al., 1984; Klein et al., 1988; Marks et al., 1990, 1991; Kuo, 1993; Sempere et al., 1997; West et al., 1997). The confinement of the AAMA within the top 120 km of the uppermost mantle beneath the AAD makes this hypothesis unlikely, however. This does not prohibit the presence of mass-preserving passive along-axis flows in response to the cool temperatures in the uppermost mantle beneath the AAD, but a cold convective current penetrating the mantle beneath the AAD does not appear consistent with the seismic evidence.

We argue that the AAMA is a stagnated remnant of a subducted slab, as argued by Gurnis et al. (1998). As shown in Figure 12, the observed temperature anomalies of up to 200°C are consistent with temperatures likely to exist in a diffusively heated slab that subducted more than 100 Ma ago. Whether this calculation is relevant to AAMA depends on the means by which the slab remnant was transported toward the surface. This calculation may reflect the thermal state of the AAMA if the anomaly detached and rose as a single piece from depth, If, however, the anomaly was extruded upwards, perhaps from a thin layer near the surface of the foundered slab in the transition zone or uppermost lower mantle, the relevance of this calculation is questionable. Whatever the nature of transport, the AAMA appears to be lying nearly horizontally in the uppermost mantle, being thinner vertically ($\sim$100 km) than in either horizontal direction ($\sim$ 500 km east-west, $\sim 2,00$ km north-south). In particular, it shows no sign of attachment to a deeper root extending into the transition zone or lower mantle. Deeper roots may have once existed and, in fact, there is evidence for their existence now (e.g., Masters et al., 200), but the AAMA is not now attached to them.

5.2 Westward migration of the AAD

If the AAMA were deeply rooted, its motion presumably would be controlled by the flow regime of the transition zone or lower mantle. Because it is not attached to a deeper root, however, the AAMA is free to move with the large-scale tectonic motions that characterize the region. Superimposed on the relative motion of Australia away from Antarctica, at a rate of about 7 cm/y, is the motion of Australia and Antarctica to the east at a speed of about 3 - 4 cm/y in the hot-spot reference frame (e.g., Gurnis et al., 1998). It is plausible that the AAMA is now moving in lock-step with these features to the east, but remains approximately fixed between Australia and Antarctica as they move apart. There is a potential problem, however, for the co-motion of the AAMA to the east with Australia and Antarctica. Gurnis et al. (1998) presents a compelling argument that, during the Cretaceous, Australia over-rode a slab that subducted at the Gondwanaland-Pacific convergent margin and foundered in the transition zone. At least during the Cretaceous, then, this slab moved independently of Australia, was deep enough in the mantle so that the Australian cratonic keel could over-ride it, and was probably controlled by a deeper mantle flow regime that differed from the surface motions of Australia. If the AAMA is a remnant of this slab, it would have only risen to its current shallow location in the uppermost mantle after it was completely over-ridden by Australia. Lin et al. (2002) discuss how the rifting of Australia off of Antarctica may have produced substantial updrafts in the uppermost mantle. These updrafts may have contributed to the ascent of the AAMA. Indeed, using 3-D convection calculations as a function of time with observed plate motions Gurnis et al. (1998) established that updrafts are expected to entrain deep seated material, and provide a mechanism of transport toward the surface. The reconstruction of Gurnis et al. (1998) places the emergence of the relict slab from beneath Australia at about 30 Ma. It is reasonable to postulate that during its ascent, the foundered slab detached from any deeper mantle roots and emerged into the large-scale flow regime of Australia, Antarctica, and the southeast Indian Ocean where it is currently suspended.

In this case, the orientation of the AAMA, trending NW-SE through the AAD, provides a simple explanation for the westward migration of the AAD based purely on plate kinematics.

If the AAD is caused by anomalously cool mantle directly beneath the spreading center, then it should originate at the intersection of the AAMA and the SEIR. The SEIR is migrating northward from Antarctica at about 3.5 cm/yr (DeMets *et al.*, 1994). If the location and orientation of the AAMA are approximately fixed in the mantle with Antarctica, the intersection of the AAMA and the SEIR would migrate westward at about 1.5 cm/yr as the SEIR moves northward, as shown in Figure 13. This is in rough agreement with the observed westward motion of the AAD (e.g., Marks et al., 1999).

5.3 The thermal and compositional state of the AAMA

We have argued that the AAMA is the suspended remnant of a slab that subducted at the Gondwanaland-Pacific convergent margin more than 100 Ma ago, foundered in the transition zone, and ascended into the shallow mantle within the past ~30 Ma. The AAMA should, therefore, be compositionally similar to subducted Pacific lithosphere, unless it underwent partial melting in the transition zone or on its ascent to the uppermost mantle. Studies of mid-ocean ridge basalts (e.g., Klein and Langmuir, 1987) and abyssal peridotites (e.g., Dick et al., 1984) reveal significant compositional variations in the upper mantle beneath mid-oceanic ridges attributed to different melting conditions beneath the ridges. Below relatively hot ridges, the degree of melting is higher and the residual mantle is more highly depleted in the basaltic component and in heavier elements, such as iron. Both geochemical data and the sea-floor depth indicate that, at present, the mantle is warmer beneath the East Pacific Rise than the SEIR (Klein and Langmuir, 1987). Therefore, the Pacific lithosphere is likely to be depleted in heavy elements compared with the Indian Ocean lithosphere. We hypothesize that the Pacific lithosphere that subducted at the Gondwanaland-Pacific convergent margin ~150 Ma ago is more similar to the present-day Pacific lithosphere than to the Indian lithosphere. Therefore, interpreting the AAMA as the remnant of old subducted Pacific lithosphere suggests that it is compositionally distinct from the surrounding Indian-type upper mantle. In particular, under this interpretation, the AAMA is likely to be depleted in heavy elements relative to the Indian Ocean lithosphere.

The stability of the AAMA and its lack of correlation with residual topography and gravity

is, therefore, attributed to near-neutral buoyancy that results from a balance between low temperatures and depletion in heavy elements, particularly iron: $\alpha\rho\Delta T \approx (\partial\rho/\partial X_{\mathrm{Fe}})\Delta X_{\mathrm{Fe}}$. Here $\alpha \approx 3.0 \times 10^{-5}\mathrm{K}^{-1}$ is the coefficient of thermal expansion (Saxena and Shen, 1992), $\rho \approx 3.3 \times 10^3$ kg/m^3 is density, ΔT is the temperature anomaly, ΔX_{Fe} is iron depletion, and $\partial\rho/\partial X_{\mathrm{Fe}} \approx 1200$ kg/m^3 (Duffy and Anderson, 1989). The bulk iron-depletion needed to balance the, on average, 100°C temperature anomalies shown in Figure 9, would, therefore, be about 0.8% with an uncertainty of about half this value. This compositional heterogeneity would have only a relatively small influence on seismic velocities: $(\partial v_s/\partial X_{\mathrm{Fe}})\,\Delta X_{\mathrm{Fe}} < 0.5\%$, if $X_{\mathrm{Fe}} < 1\%$, taking the partial derivative from Goes et al. (2000).

Although Johnson et al. (1990) show that iron/magnesium ratios may vary between individual samples of abyssal peridotites by up to 3%, Dick et al. (1984) present evidence for aggregated trends in iron content between ridge segments in the Indian and Atlantic Oceans to be a little more than 1%. A bulk iron depletion of 0.8% within the AAMA may, therefore, be somewhat higher than is likely to occur. If the temperature anomalies in Figure 9 are overestimated, however, then the requisite iron-depletion would be proportionally reduced.

We conclude that the AAMA is approximately neutrally buoyant and the average temperature depression within the AAMA is probably somewhat less than 100°C. The thermally induced density anomaly is approximately balanced by the bulk depletion in iron of <0.8%.

Previous estimates of temperature anomalies beneath the AAD segregate according to the method used, with geophysically (largely seismically) determined temperature depressions typically being larger (100°C - 250°C) than those estimated geochemically (60°C - 150 °C). Figure 9 may illuminate the cause of this difference: the largest temperature anomalies do not reside in the shallowest mantle. As argued by West et al. (1997), the geochemical estimates reflect temperatures in the melting region which is in the shallowest mantle. We estimate that the average temperature anomaly in the upper mantle beneath the AAD is probably no larger than 100°C, but the temperature depression in the shallowest mantle is less than this average and the maximum temperature depression, which lies at about 60 km depth in our model, is substantially greater.

5.4 Crustal formation and residual topography

Geochemical evidence (e.g., Klein et al., 1991) establishes the AAD as a region with a low degree of partial melting as well as lower melt production and supply, and agrees with seismic evidence (Tolstoy et al., 1995) that the crust is thin. It is likely that the depressed temperatures within the AAMA inhibit melt production and provide the root cause of these phenomena, at least in a large-scale spatially averaged sense. The poor correlation between the AAMA with residual topography off the SEIR implies that topographic anomalies, both along the SEIR and off-axis, owe their existence to processes involved in the formation of the crust. Because processes of crustal formation occur at spatial scales much smaller than the resolution of our model, we do not anticipate a detailed correlation between the complex of topographic features that exist along the SEIR (ridge segmentation, chaotic topography, propagating ridges, etc.) with the AAMA. In a spatially averaged sense, however, we believe that residual depth anomalies are locally compensated by thinned crust and perhaps very light uppermost mantle and, in particular, do not result from convective down-welling because the AAMA is approximately neutrally buoyant. Gurnis et al. (2000), in a comprehensive discussion about crustal formation and mantle temperatures from a dynamical modeling standpoint, argue that about half of the residual topography results from crustal thinning. Our evidence suggests, however, that topography is essentially controlled by crustal thinning, at least at the spatial scales of the seismic model.

The 800 m of anomalous topography relative to adjoining ridge segments, therefore, would require crustal thinning of about 4.5 km. Although this is somewhat larger than reported by Tolstoy et al. (1995), using the arguments of Langmuir et al. (1992) who estimate the crust will thin by about 60 meters for each 1°C decrease in average mantle temperature beneath the ridge, the temperature anomalies shown in Figure 9 are in general agreement with this value. For example, at 122°E the average temperature depression in the top 175 km beneath the ridge is about 80°C relative to the adjacent ridge segments outside the AAD. These cool temperatures would generate about 4.8 km of crustal thinning using the methods from Langmuir et al. (1992).

The uncertainties in each of the values used in this calculation (amplitude of temperature anomaly, depth interval of integration, partial derivative of crustal thickness with respect to temperature anomaly) are too large to give the results much credence, but we believe these calculations do establish the reasonableness of the hypothesis that at large spatial scales crustal thickness controls the residual depth anomaly. Resolution of this issue will await more extensive seismic studies performed in the neighborhood of the AAD to estimate crustal thickness.

In our view, therefore, residual topography originates at the intersection of the AAMA with the SEIR due to inhibition of crustal formation. As discussed in section 5.2, the northward migration of the SEIR causes the AAD to move northwest along the strike of the AAMA (i.e., west in the frame of the ridge). As a result, as new crust forms the depth anomaly will move off the ridge-axis, producing a V-shaped "wake" in the bathymetry of the southeast Indian Ocean as the AAD migrates westward along the SEIR. This is illustrated in Figure 13b.

Aspects of this argument were foreseen by Klein et al. (1988) and Gurnis et al. (1998) who discussed the effect of the SEIR ridge moving north over a "cold-line" in the mantle. The cold-line for Klein et al. was a convective down-welling and for Gurnis et al. it was a relict slab, but both imagined the feature oriented north-south through the AAD, for want of better information. Gurnis et al. hypothesized that the westward migration of the AAD and the V-shaped residual depth anomaly result from the motion of Australia and Antarctica to the east in the hotspot reference frame while the cold-line remained approximately fixed. Others have argued that these features result from the westward migration of Pacific Ocean asthenosphere into Indian Ocean asthenosphere (e.g., Lanyon et al., 1995). These are essentially the same argument presented from different frames of reference – the hotspot frame and the frame of the SEIR, respectively. We have argued above, however, that the AAMA is very shallow and is detached from deeper roots, so it is co-moving with Australia and Antarctica to the east with respect to the hot-spot frame. The V-shaped residual topography, therefore, does not require the invasion of Pacific oceanic asthenosphere into the Indian oceanic asthenosphere from the east. It results rather from the formation of anomalously thin crust at the intersection of the AAMA and the SEIR, the northward migration of the SEIR, and the

NW-SE orientation of the AAMA, which could not have been foreseen by previous researchers.

5.5 Consequences on mantle flow and a geochemical province boundary

The existence of a 500 km × 1500 km cold mantle anomaly in the uppermost mantle that is compositionally distinct from the surrounding lithosphere will affect mantle flow. Although significant progress has been made in simulating the dynamical conditions that formed the AAD (e.g., West et al., 1997; Gurnis et al., 1998; Gurnis et al., 2000; Gurnis and Müller, 2003; Lin et al., 2002), full understanding of large-scale convection between Australia and Antarctica will await dynamical simulations that model the origin and effects of the AAMA, including its geometry and depth extent. In lieu of these models, three observations are worth noting. First, although the compositional anomaly will probably have little dynamical effect, by increasing viscosity the cool temperatures will tend to inhibit flows through the AAMA beneath the AAD. As a consequence, the AAMA will act as a barrier to east-west flows within the upper asthenosphere and may, indeed, mark a mantle convection boundary as proposed by Klein et al. (1988), although the boundary will not be characterized by a down-welling. The boundary will exist not only at the AAD, but will also extend NW-SE through the AAD along the strike of the AAMA. Second, although the AAMA will obstruct east-west flows, its westward dip may also affect the passive transport of asthenospheric material to the AAD. Figure 9 reveals that mantle temperatures are cooler toward the east end of the AAD, as isotherms generally dip to the west. Along-axis flows in the asthenosphere will be more efficiently obstructed from the Pacific Ocean side, yielding predominant along-axis asthenospheric flows from the west. This may contribute to Indian Mid-Ocean Ridge Basalts (MORBs) penetrating nearly to the eastern end of the AAD. Christie et al. (2001) have shown that the Indian - Pacific geochemical boundary follows the eastern side of the AAD depth anomaly along the SEIR. Third, as a boundary to convection, the AAMA may also mark a boundary separating Pacific and Indian type geochemical provinces. Although the AAMA may be the province boundary in the mantle, the isotopic distribution observed in basalts will approximately follow a V-shaped trend similar to the residual depth anomalies. This is consistent with the observation that the Indian-Pacific isotopic boundary does not continue directly northward from the AAD (e.g.,

Lanyon et al., 1995). North and east of the AAD, then, Indian Ocean MORBs may, in fact, overlie Pacific type mantle, as shown in Figure 14. In any event, in this region one needs to be careful in inferring mantle geochemistry from the overlying MORBs.

The relevance of some of these comments depends on the extent to which the large-scale features of the AAMA affect magma generation and transport. If magma transport is largely in the shallowest mantle and is strongly affected by structures such as ridge-segmentation that are not resolvable in the seismic model, then the large-scale seismic model may be of limited help in unraveling the details of the distribution of MORBs across the southeast Indian Ocean. In addition, as it currently appears (e.g. Pyle et al., 1995), the MORB boundary and the residual depth anomaly that marks the locus of points that were once at the AAD, may not coincide. This may be because mantle structures with different length scales and that occur at different depths affect topography and basalt chemistry differently. Nevertheless, more complete sampling of MORBs across the southeast Indian Ocean is crucial in helping to determine the effect of the AAMA on the convective state of the upper mantle.

Acknowledgments

This paper benefited from critical reviews from David Christie, Michael Gurnis, and Ban-Yuan Kuo. We would like to thank the staffs of the IRIS-DMC and the GEOSCOPE data center for providing most of the waveform data on which the dispersion measurements were obtained. We thank Shi-Jie Zhong for many valuable conversations. We are also particularly grateful to Jeannot Trampert at Utrecht University and Michael Antolik, Adam Dziewonski, and Goran Ekström at Harvard University for providing phase speed measurements and to Robert van der Hilst and Brian Kennett for donating waveform data from the SKIPPY and KIMBA arrays in Australia. The SKIPPY and KIMBA data-sets were collected by the Research School of Earth Sciences, Australian National University, and greatly improved the quality of the dispersion maps at short and intermediate periods. All maps were generated with the Generic Mapping Tools (GMT) data processing and display package (Wessel and Smith, 1991, 1995). This work was supported by grants from the Office of Polar Programs at

the U.S. National Science Foundation, NSF-OPP-9615139 and NSF-OPP-0125848.

References

Barmin, M.P., M.H. Ritzwoller, A.L. Levshin, A fast and reliable method for surface wave tomography, *Pure Appl. Geophys., 158*, 1351-1375, 2001.

Christie, D.M., R.B. Pedersen, D.J. Miller, et al., Mantle Reservoirs and Migration Associated with Australian-Antarctic Rifting, *Proc. ODP, Init. Repts., 187*, College Station, TX (Ocean Drilling Program), 2001.

DeMets, C., R.G. Gordon, D.F. Argus, and S. Stein, Effect of recent revisions to the geomagnetic reversal time scale on estimates of current plate motions, *Geophys. Res. Lett., 21*, 2191-2194, 1994.

Dick, H.J.B., R.L. Fisher, and W.B. Bryan, Mineralogic variability of the uppermost mantle along mid-oceanic ridges, *Earth Planet. Sci. Lett. 69*, 88-106, 1984.

Duffy, T.S. and D.L. Anderson, Seismic velocities in mantle minerals and the mineralogy of the upper mantle, *J. Geophys. Res., 94*, 1895-1912, 1989.

Dziewonski, A.M., and D.L. Anderson, Preliminary Reference Earth Model, *Phys. Earth Planet. Int., 25*, 297-356, 1981.

Ekström, G., J. Tromp, and E.W.F. Larson, Measurements and global models of surface waves propagation, *J. Geophys. Res. 102*, 8137-8157, 1997.

Forsyth, D.W., R.L. Ehrenbard, and S. Chapin, Anomalous upper mantle beneath the Australian-Antarctic Discordance, *Earth Planet. Sci. Lett. 84*, 471-478, 1987.

Forsyth, D.W., Geophysical constraints on mantle flow and melt generation beneath mid-ocean ridges, *Mantle Flow and Melt Generation at Mid-Ocean Ridges, Geophys. Monogr. Ser., 71*, ed. by J. Phipps Morgan, D. Blackman, and J. Sinton, pp. 1-65, AGU, Washington, D.C., 1992.

Goes, S., R. Govers, and P. Vacher, Shallow mantle temperatures under Europe from P and S wave tomography, *J. Geophys. Res. 105*, 11153-11169, 2000.

Gurnis, M. and R.D. Müller, The origin of the Australian-Antarctic Discordance from an ancient slab and mantle wedge, *The Evolution and Dynamics of the Australian Plate*, Geological Society of Australia Special Publication *22*, 422-423, 2003.

Gurnis, M., R.D. Müller, and L. Moresi, Cretaceous vertical motion of Australia and the Australian-Antarctic Discordance, *Science, 279*, 1499-1504, 1998.

Gurnis, M., L. Moresi, and R.D. Müller, Models of mantle convection incorporating plate tectonics: The Australian region since the Cretaceous, in M.A. Richards, R. Gordon, and R. van der Hilst (eds.), The History of Global Plate Motions, Am. Geophys. Un., Washington, D.C., 211-238, 2000.

Hayes, D.E., Nature and implications of asymmetric sea-floor spreading - Different rates for different plates, *Geol. Soc. Am. Bull., 87*, 994-1002, 1976.

Hayes, D.E., Age-depth relationships and depth anomalies in the southeast Indian Ocean and South Atlantic Ocean, *J. Geophys. Res., 93*, 2937-2954, 1988.

Johnson, K.T., H.J.B. Dick, and N. Shimizu, Melting in the oceanic upper mantle: An ion microprobe study of diopsides in abyssal peridotites, *J. Geophys. Res., 95*, 2661-2678, 1990.

Kennett, B.L.N., E.R. Engdahl, and R. Buland, Constraints on seismic velocities in the Earth from travel times, *Geophys. J. Int., 122*, 108-124, 1995.

Klein, E.M. and C.H. Langmuir, Global correlation of ocean ridge basalt chemistry with axial depth and crustal thickness, *J. Geophys. Res. 92*, 8089-8115, 1987.

Klein, E.M., C.H. Langmuir, A. Zindler, H. Staudigel, and B. Hamelin, Isotope evidence of a mantle convection boundary at the Australian-Antarctic Discordance, *Nature, 333*, 623-629, 1988.

Klein, E.M., C.H. Langmuir, and H. Staudigel, Geochemistry of basalts from the southeast Indian Ridge, 115°E -138°E, *J. Geophys. Res., 96*, 2089-2107, 1991.

Kuo, B.-Y., Thermal anomalies beneath the Australian-Antarctic discordance, *Earth Planet. Sci. Lett. 119*, 349-364, 1993.

Kuo, B.-Y., C.-H. Chen, and Y.-S. Zhang, A fast velocity anomaly to the west of the Australian-Antarctic Discordance, *Geophys. Res. Lett., 23*, 2239-2243, 1996.

Langmuir, C.H., E.M. Klein, and T. Plank, *Mantle Flow and Melt Generation at Mid-Ocean Ridges, Geophys. Monogr. Ser., 71*, ed. by J. Phipps Morgan, D. Blackman, and J. Sinton, pp. 183-280, AGU, Washington, D.C., 1992.

Lanyon, R., A.J. Crawford, S.M. Eggins, Westward migration of the Pacific Ocean upper mantle into the Southern Ocean region between Australia and Antarctica, *Geology, 23*, 511-514, 1995.

Levshin, A.L., M.H. Ritzwoller, and J.S. Resovsky, Source effects on surface wave group travel times and group velocity maps, *Phys. Earth Planet. Int. 115*, 293-312, 1999.

Lin, S.-C., L.-Y. Chiao, and B.-Y. Kuo, Dynamic interaction of cold anomalies with the mid-ocean ridge flow field and its implications for the Australian-Antarctic Discordance, *Earth Planet. Sci. Lett., 203*, 925-935, 2002.

Marks, K.M., P.R. Vogt, and S.A. Hall, Residual depth anomalies and the origin of the Australian-Antarctic Discordance, *J. Geophys. Res., 95*, 17,325-17,338, 1990.

Marks, K.M., D.T. Sandwell, P.R. Vogt, and S.A. Hall, Mantle downwelling beneath the Australian-Antarctic Discordance zone: Evidence from geoid height versus topography, *Earth Planet. Sci. Lett., 103*, 325-338, 1991.

Marks, K.M., J.M. Stock, and K.J. Quinn, Evolution of the Australian-Antarctic Discordance since Miocene time, *J. Geophys. Res. 104*, 4967-4681, 1999.

Masters, G., G. Laske, H. Bolton, and A. Dziewonski, The relative behavior of shear velocity, bulk sound speed, and compressional velocity in the mantle: Implications for chemical and thermal structure, in *Earth's Deep Interior: Mineral Physics and Tomography from the Atomic to the Global Scale*, ed. S. Karato, A. Forte, R.C. Liebermann, G. Masters, and L. Stixrude, Geophysical Monograph 117, 63-87, Amer. Geophys. Un., 2000.

Müller, R.D., W.R. Roest, J.-Y. Royer, L.M. Gahagan, and J.G. Sclater, Digital isochrons of the world's ocean floor, *J. Geophys. Res., 102*, 3211-3214, 1997.

Pyle, D.J, D.M. Christie, J.J. Mahoney, and R.A. Dunkan, Geochemistry and geochronology of ancient southeast Indian and southwest Pacific sea floor, *J. Geophys. Res., 100*, 22,261-22,282, 1995.

Ritzwoller, M.H. and A.L. Levshin, Eurasian surface wave tomography: Group velocities, *J. Geophys. Res., 103*, 4839-4878, 1998.

Ritzwoller, M.H., N. Shapiro, A. Levshin, and G.M. Leahy, Crustal and upper mantle structure beneath Antarctica and surrounding oceans, *J. Geophys. Res., 106*, 30,645-30,670, 2001.

Ritzwoller, M.H., N. Shapiro, M.P. Barmin, and A.L. Levshin, Global surface wave diffraction tomography, *J. Geophys. Res., 107(B12)*, 2335, 2002.

Saxena, S.K. and G. Shen, Assessed data on heat capacity, thermal expansion, and compressibility from some oxices and silicates, *J. Geophs. Res., 97*, 19,813-19.825, 1992.

Sempere, J.-C. , J.R. Cochran, and the SEIR scientific team, The Southeast Indian Ridge between 88°E and 118°E: variations in crustal accretion at constant spreading rate, *J. Geophys. Res., 102*, 15463-15487, 1997.

Shapiro, N.M., and M.H. Ritzwoller, Monte-Carlo inversion of broad-band surface wave dispersion for a global shear velocity model of the crust and upper mantle, *Geophys. J. Int.*, 151, 88-105, 2002a.

Shapiro, N.M. and M.H. Ritzwoller, Thermodynamic constraints on seismic inversions, Geophys. J. Int., submitted, 2003.

Shen, Y. and D.W. Forsyth, Geochemical constraints on initial and final depths of melting beneath mid-ocean ridges, *J. Geophys. Res., 100*, 2211-2237, 1995.

Smith, W. H. F., and D. T. Sandwell, Global seafloor topography from satellite altimetry and ship depth soundings, Science, 277, 1957-1962, 1997.

Tolstoy, M., A.J. Harding, J.A. Orcutt, and J. Phipps Morgan, Crustal thickness at the Australian-Antarctic discordance and neighboring Southeast Indian Ridge, *EOS Trans. AGU, Fall Meet. Suppl. 76(46)*, F570, 1995.

Trampert, J. and J.H. Woodhouse, Global phase velocity maps of Love and Rayleigh waves between 40 and 150 s period, *Geophys. J. Int. 122*, 675-690, 1995.

Veevers, J.J., Australian-Antarctic depression from the mid-ocean ridge to adjacent continents, *Nature, 295*, 315-317, 1982.

Vogt, P.R., N.K. Cherkis, an G.A. Morgan, Project Investigator, Evolution of the Australian-Antaractic Discordance from a detailed aeromagnetic study, in *Antarctic Earth Science: Proceedings of the 4th International Symposium on Antarctic Earth Sciences*, ed. R.L. Oliver, P.R. James, and J. Jago, pp. 608-613, Aust. Acad of Sci., Canberra, 1984.

Weissel, J.K., and D.E. Hayes, Asymmetric spreading south of Australia, *Nature, 213*, 518-521, 1971.

Weissel, J.K., and D.E. Hayes, The Australian-Antarctic Discordance: New Results and Implications, *J. Geophys. Res., 79*, 2579-2588, 1974.

Wessel, P., and W.H.F. Smith, Free software helps map and display data, *Eos, Trans. Am. Geophys. Un., 72*, 441, 1991.

Wessel, P., and W.H.F. Smith, New version of the Generic Mapping Tools released, *Eos, Trans. Am. Geophys. Un., 76*, 329, 1995.

West, B.P., W.S.D. Wilcock, J.-C. Sempéré, and L. Géli, Three-dimensional structure of asthenospheric flow beneath the Southeast Indian Ridge, *J. Geophys. Res. 102*, 7783-7802, 1997.

Zhang, Y.S. and T. Tanimoto, High resolution global upper mantle structure and plate tectonics, *J. Geophys. Res. 98*, 9783-9823, 1993.

Received _____

Table 1. χ-misfit (eqn. (1)) to the dispersion curves at the AAD (Figure 3).

model	*all data*	*Rayleigh only*	*Ralyeigh group only*
1 Ma†	1.80	1.82	2.21
5 Ma†	1.50	1.51	1.81
10 Ma†	1.29	1.29	1.53
20 Ma†	1.15	1.24	1.15
30 Ma†	1.95	2.20	1.77
40 Ma†	2.76	3.07	2.45
ensemble spread††	0.97 - 1.40	1.06 - 1.75	0.89 - 1.64
median model†††	1.13	1.26	1.02

† – age-dependent models.

†† – range from the full ensemble of acceptable models at the AAD.

† † † – ensemble median model at the AAD.

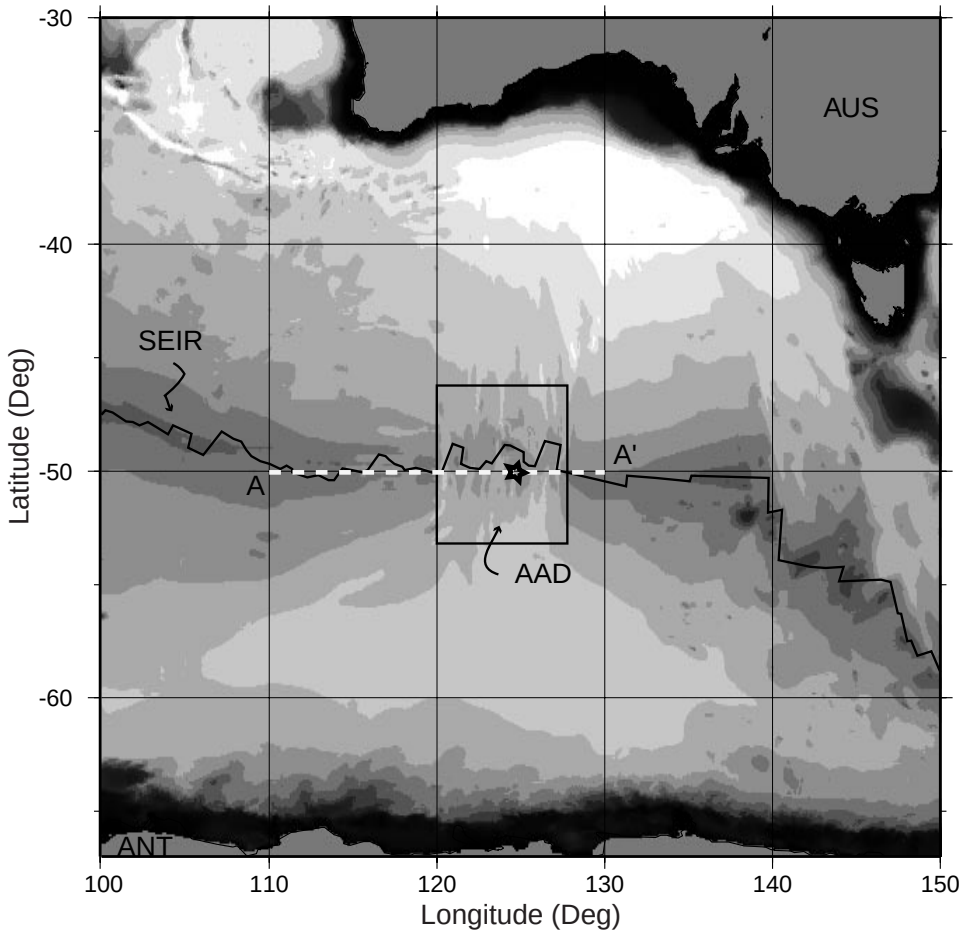

Figure 1. Bathymetric reference map of the Southeast Indian Ocean (Smith and Sandwell, 1997). The Australian-Antarctic Discordance (AAD) region is boxed. The Southeast Indian Ridge (SEIR) cuts across the center of the figure. The star (50°S, 124°E) marks the location of the 1-D model shown in Figures 3 and 4.

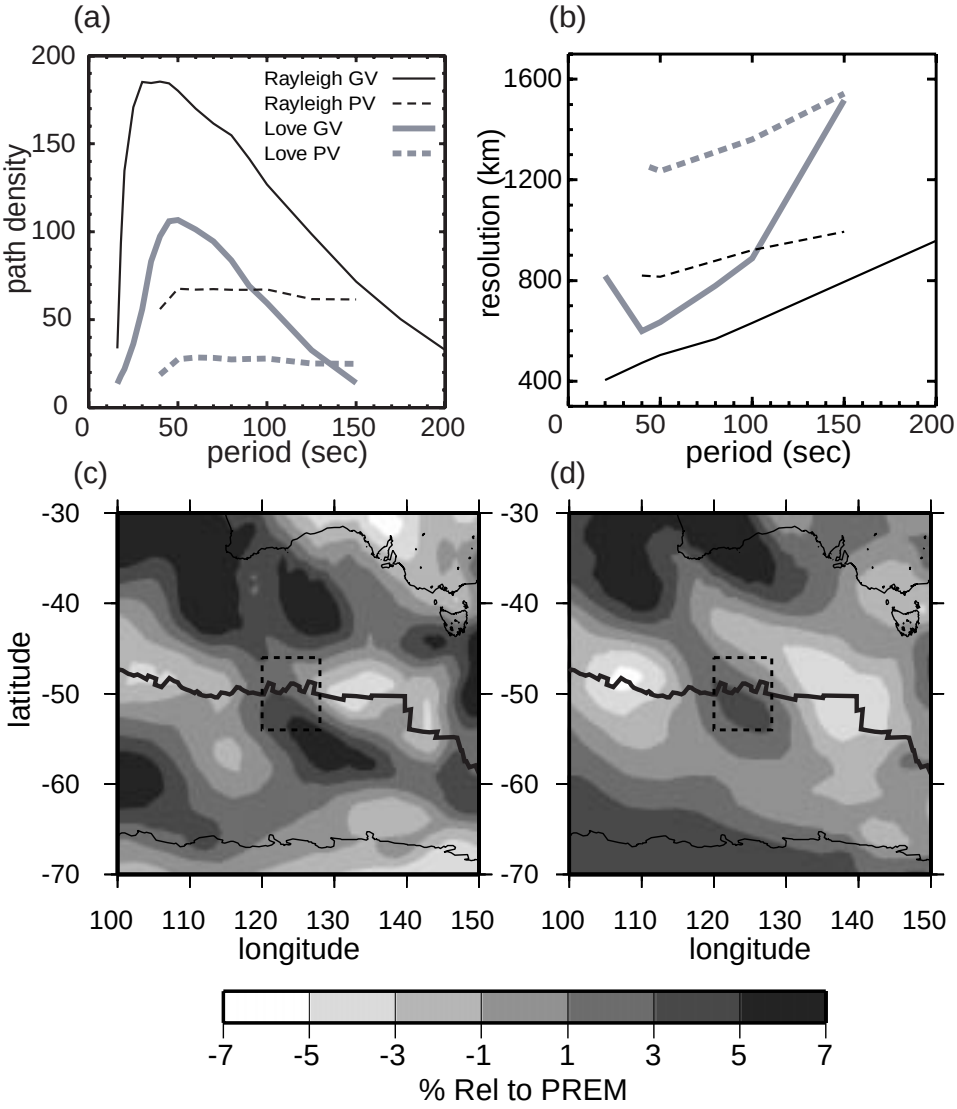

Figure 2. (a) Path density averaged over the region of study, presented as the number of paths crossing each $2^\circ \times 2^\circ$ cell (GV: group velocity, PV: phase velocity). (b) Estimated resolution averaged over the region of study. Line definition is as in (a). (c)-(d) Rayleigh wave group velocity maps shown as perturbations relative to PREM (Dziewonski and Anderson, 1981) at 45 sec (c) and 70 sec (d) period.

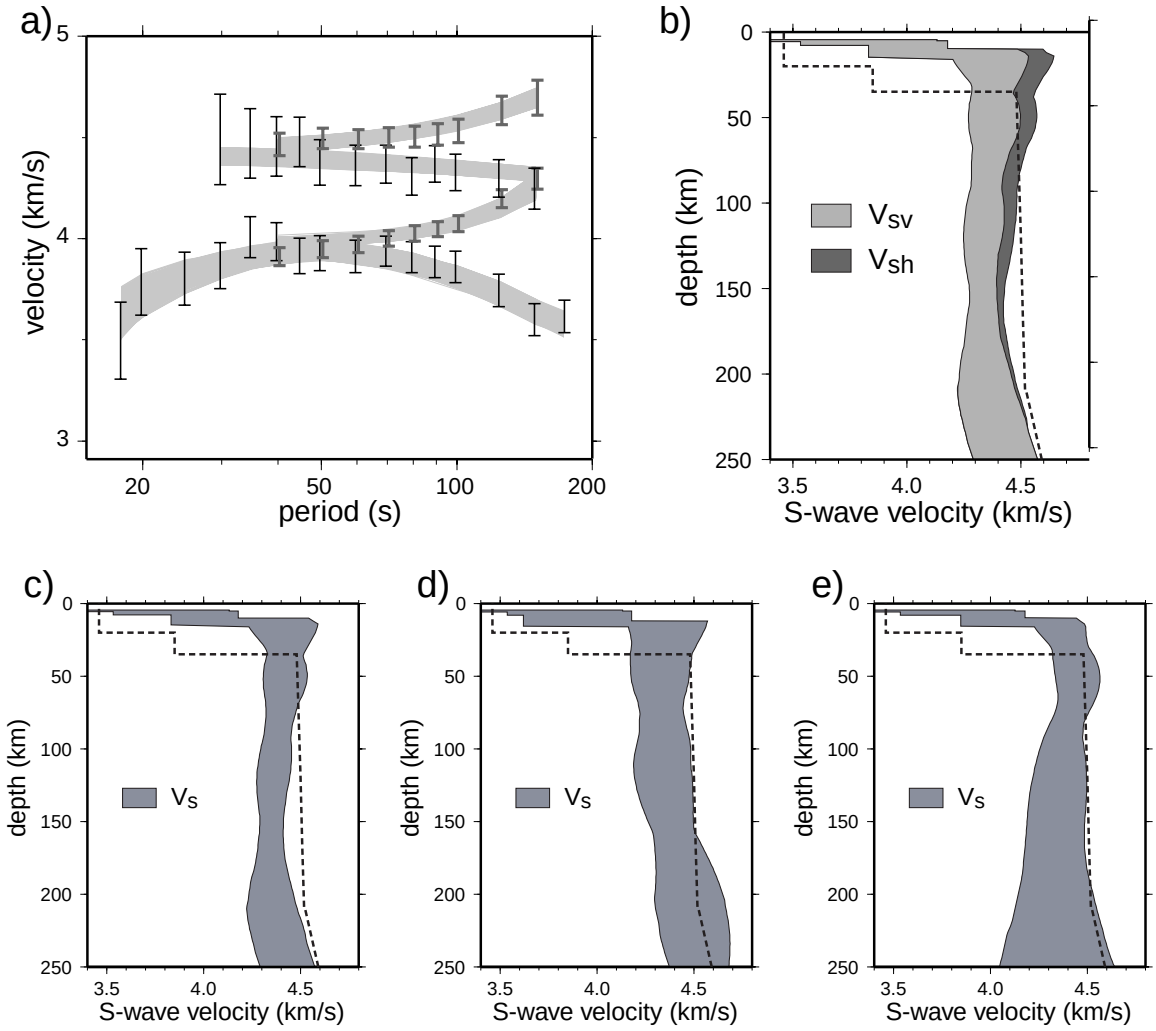

Figure 3. (a) Dispersion measurements presented as 2σ error bars obtained at the starred point in Figure 1. Dispersion curves resulting from the ensemble of acceptable models (Figure 3b) are overplotted as grey lines. (b) The ensemble of acceptable models that emerge from the Monte-Carlo inversion of the group and phase speed curves. The dashed line is V_s from the 1-D model ak135 (Kennett et al., 1995). (c) Ensemble of isotropic models derived from inverting group and phase speeds simultaneously, taken from the ensemble in Figure 3b where $V_s = (V_{sh} + V_{sv})/2$). (d) Same as Figure 3c, but only the phase speeds are used. (e) Same as Figure 3c, but only the group speeds are used.

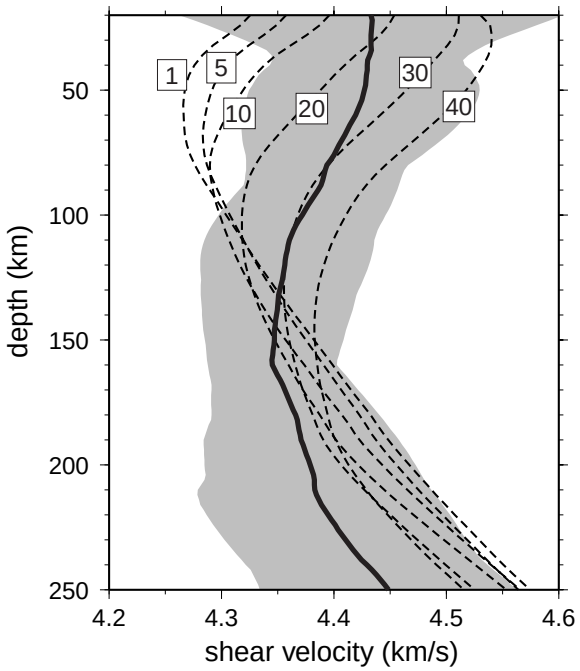

Figure 4. Age-dependent shear velocity models averaged over lithospheric age provinces in the southeast Indian Ocean are plotted as dashed lines with lithospheric ages indicated in Ma. The corridor defining the ensemble of acceptable isotropic models at the AAD (the starred point in Figure 1) is presented in grey, similar to Figure 3c. The ensemble median model at this point is shown as the bold solid line.

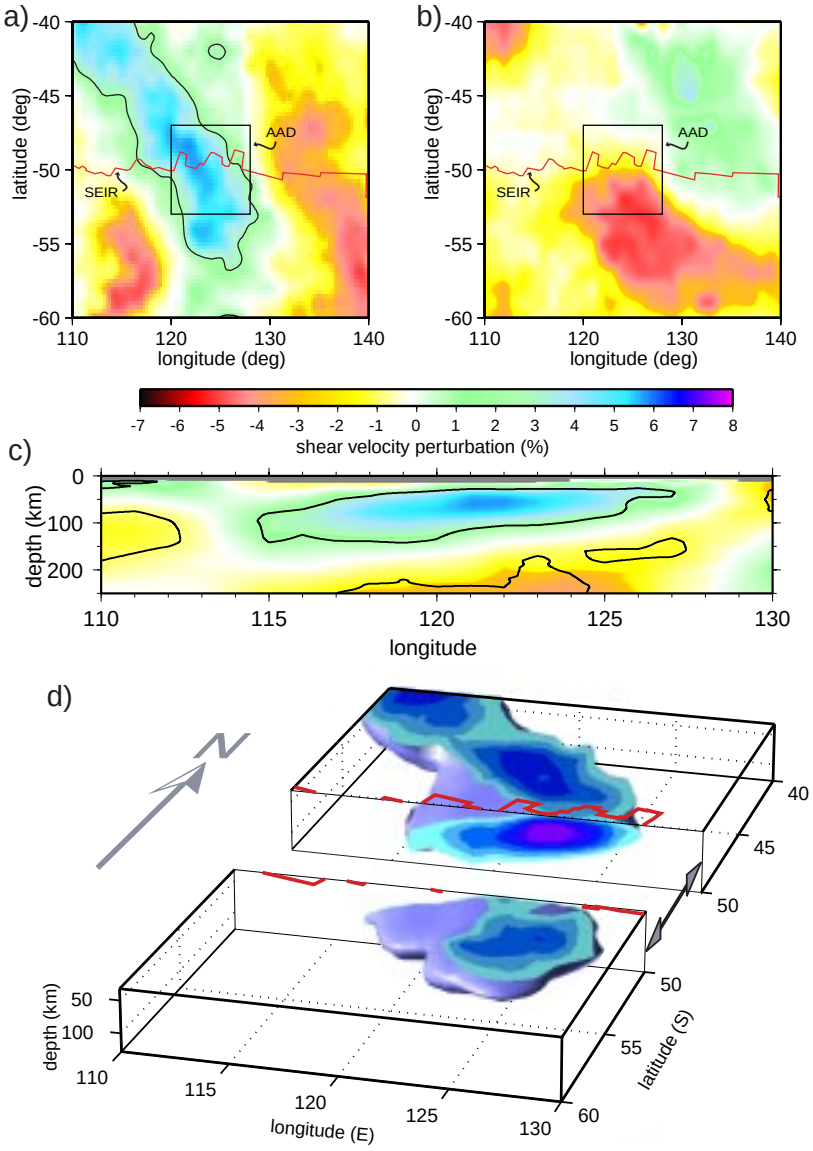

Figure 5. Images of the AAMA. (a) Horizontal slice of the V_s model at 60 km depth plotted with respect to the age-dependent model, selected age profiles of which are shown in Figure 4. Black contours indicate +3% perturbations. (b) Similar to (a), but at 200 km depth. (c) Vertical slice of the V_s model along path A - A' (Figure 1) relative to the 1 Ma age average. Black contour shows the persistent features of the model. (d) Isosurface (+2%) representation of the AAMA relative to the age-dependent model. The model was spatially smoothed somewhat to highlight the dominant large-scale features, which trend in the NW-SE direction and extend no deeper than about 120 km.

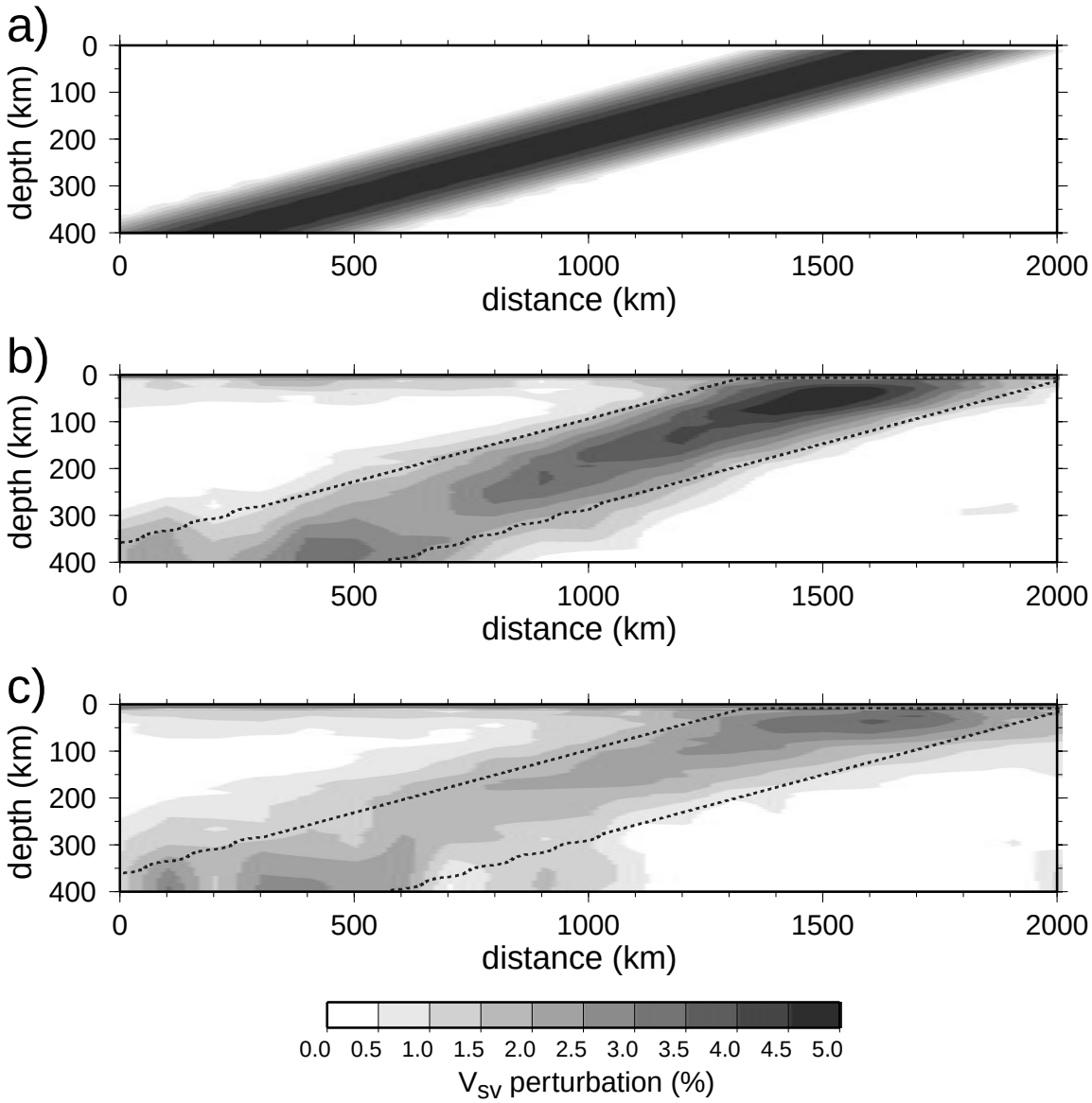

Figure 6. Synthetic resolution test. (a) Synthetic input model of a high velocity anomaly extending into the transition zone. This perturbation is taken relative to the 1 Ma age model. (b) Model estimated with the Monte-Carlo inversion of the synthetic phase and group velocities computed from the model in (a). (c) Model estimated from synthetic phase and group velocity maps that have been smoothed laterally to match the estimated period and wave type dependent resolution (Figure 2b). The dotted lines in (b) and (c) outline the input structure.

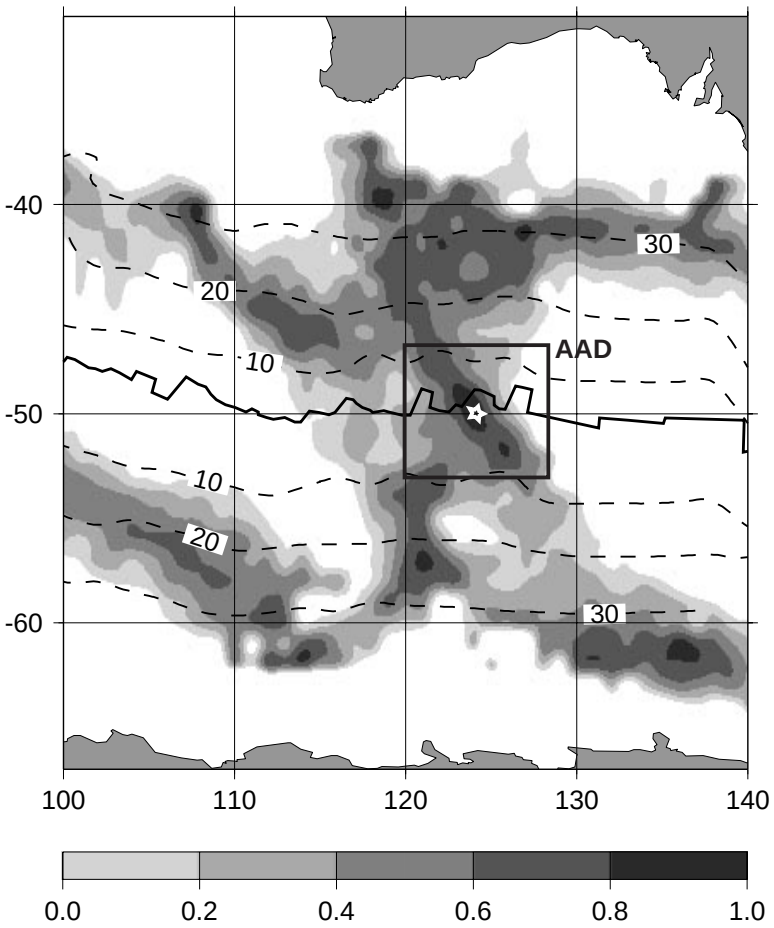

Figure 7. Similarity, defined by equation (2), between the mantle model beneath the AAD (starred point) and the rest of the southeast Indian Ocean upper mantle. Darker grey shades indicate stronger similarity to the mantle beneath the AAD. Lithospheric age isochrons are shown as dashed lines. Results are for the model with the seismic parameterization.

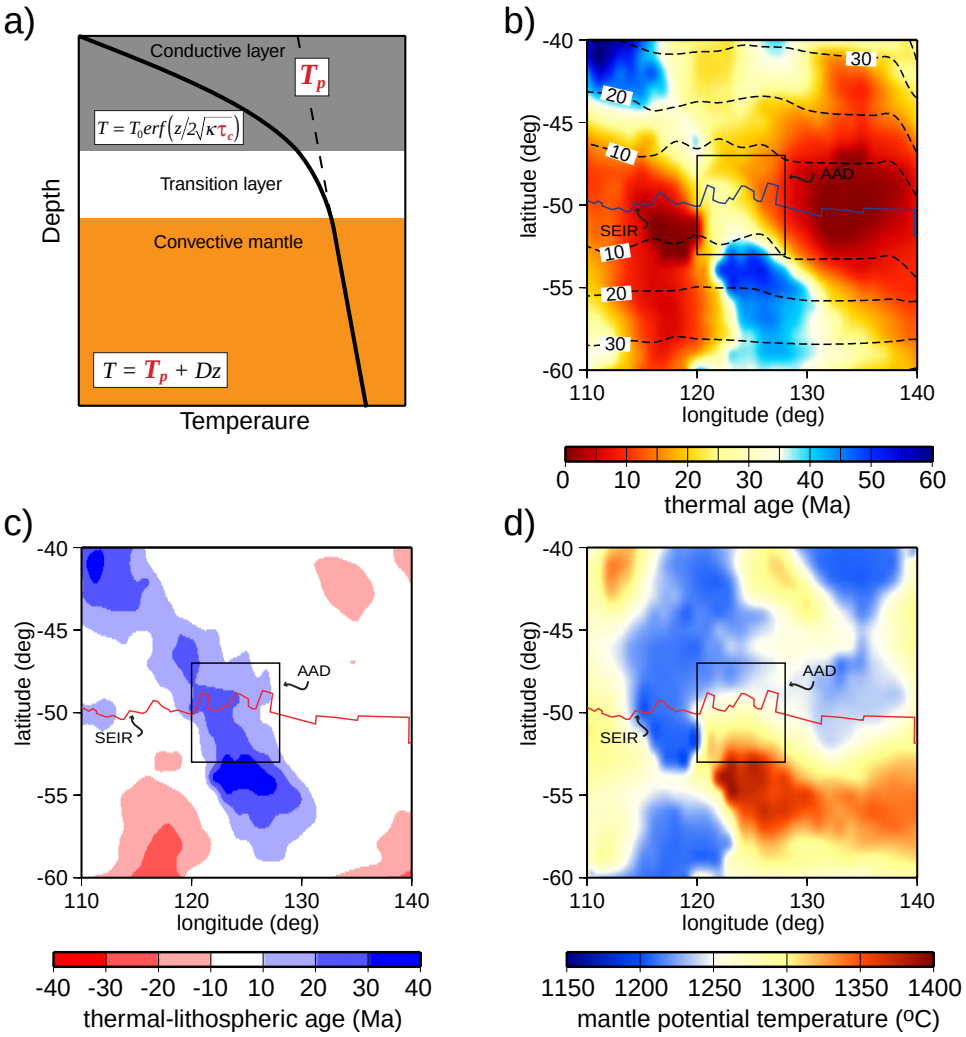

Figure 8. Results of the inversion with the thermal parameterization of the oceanic lithosphere, for comparison with results using the seismic parameterization. (a) The thermal parameterization is defined by a conductive layer, described by thermal age τ_c, underlain by a convecting asthenosphere described by the mantle adiabat which is represented by potential temperature T_p. (b) Estimated apparent thermal age, τ_c, across the southeast Indian ocean lithosphere. Isochrons of lithospheric ages are overplotted as dashed lines. (c) Difference between thermal age and lithospheric age. The entire AAMA, including the region of the AAD, is much cooler than its lithospheric age would suggest. (d) Estimated mantle potential temperature, T_p, of the southeast Indian ocean asthenosphere.

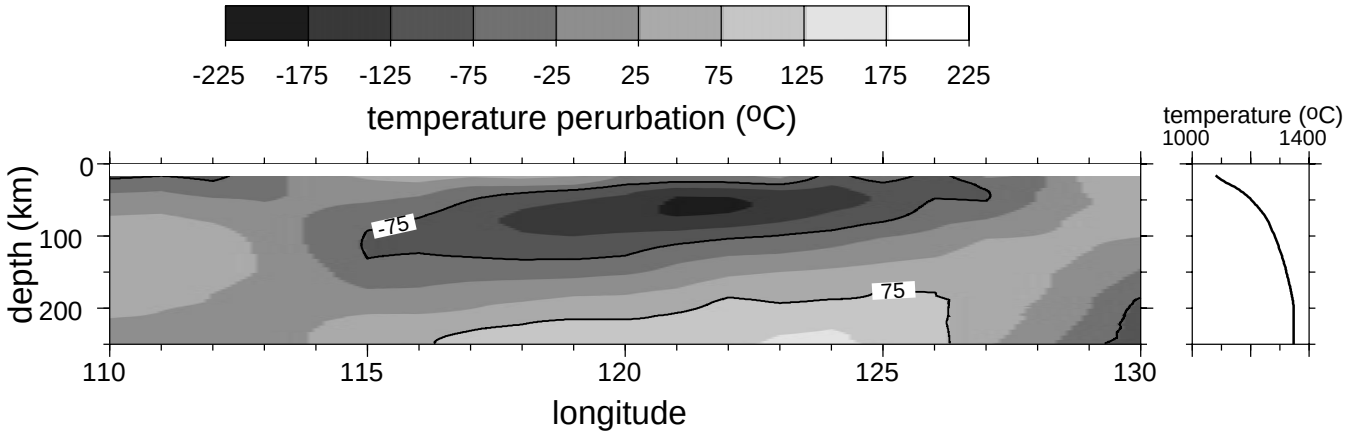

Figure 9. Temperature variations beneath profile $A - A'$ in Figure 1, taken relative to the average temperature profile along the SEIR, shown at right. Temperatures are computed from the model with the seismic parameterization shown in Figure 5c.

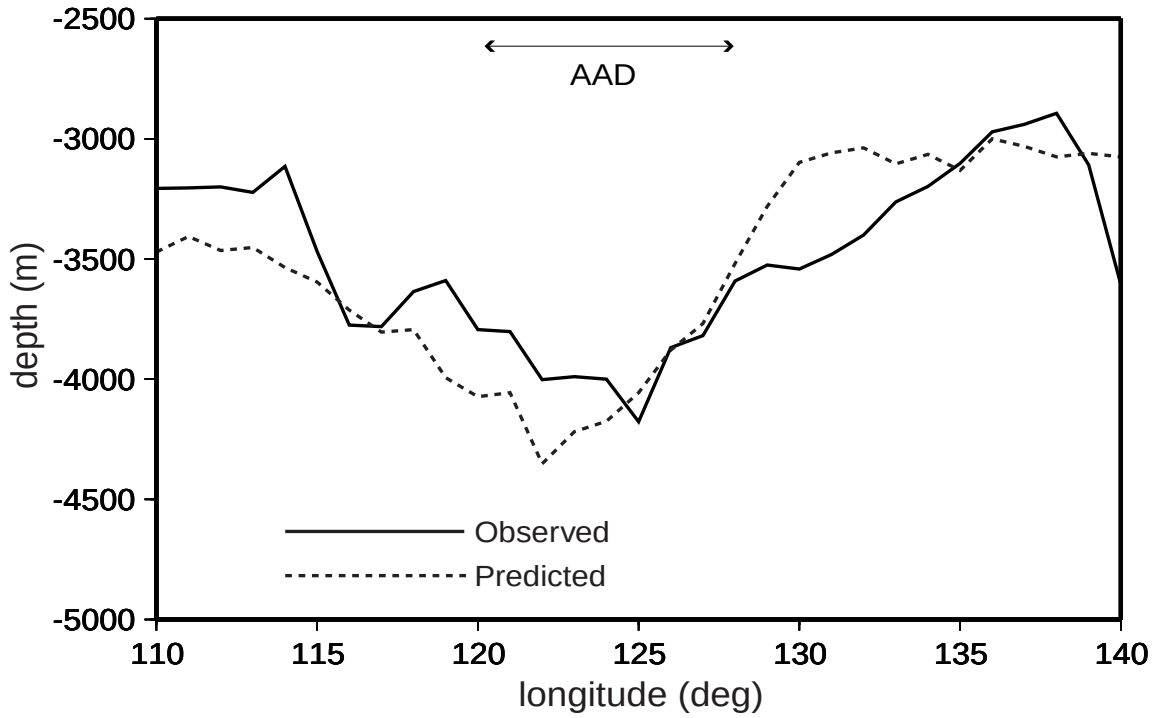

Figure 10. Comparison between the observed topography along profile $A - A'$ in Figure 1 and that predicted assuming isostatic compensation from the temperature model shown in Figure 9 The predicted topography has been shifted vertically to match the average observed topography. Results are for the model with the seismic parameterization.

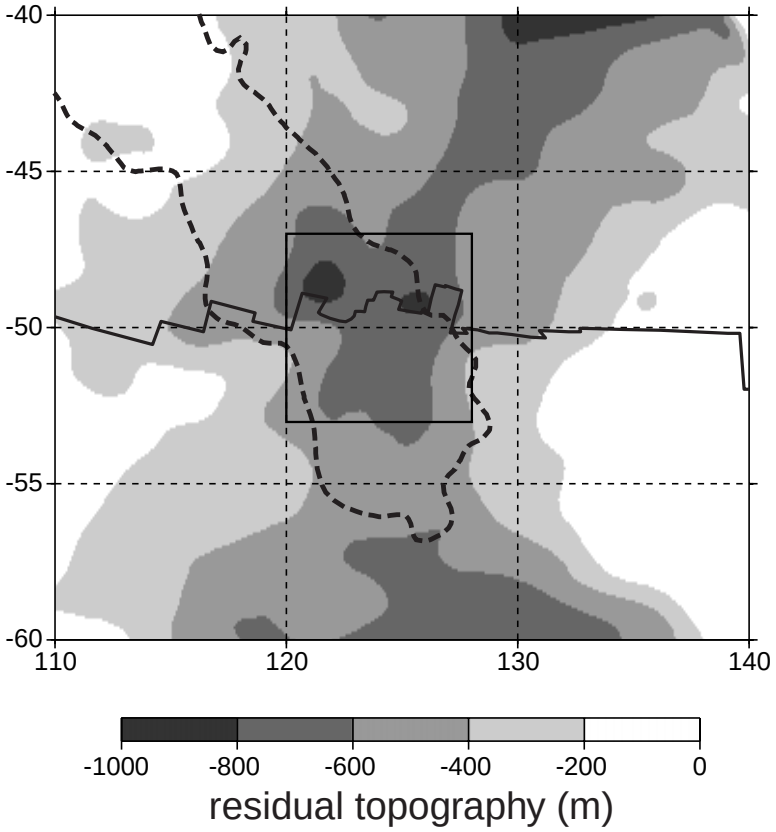

Figure 11. Residual topography (dh) compared with the 3% contour (dashed line) of the AAMA at 60 km depth (taken from Figure 5a). Residual topography is the difference between the topography estimated by Smith and Sandwell (1997), which we refer to as "observed", and topography predicted from sea floor age A in Ma: $dh = 2620$ m - $350\sqrt{A}$ m. Both the observed and predicted topography are smoothed using a spatial Gaussian filter with a standard deviation of 70 km. The observed topography is corrected isostatically for sedimentary load taken from the crustal model of Laske and Masters (2002, personal communication). The residual depth anomaly (dark grey shades) forms a V-shaped feature that is poorly correlated with the AAMA except at the SEIR.

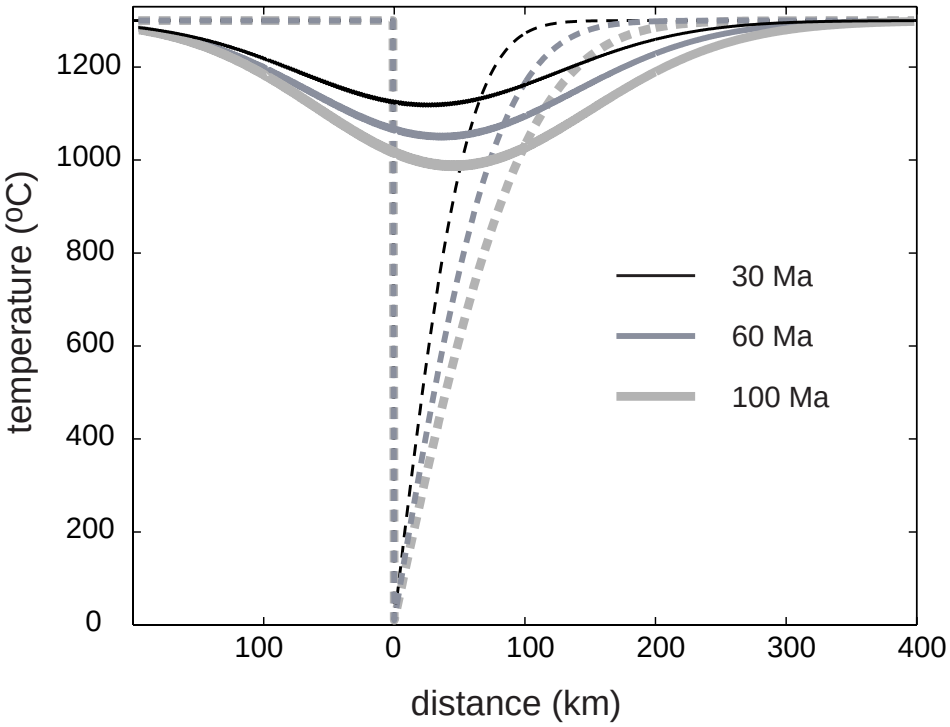

Figure 12. Initial and final temperature profiles for a 1-D slab heated diffusively along two sides. Dashed lines are the initial temperature profiles (error functions) for oceanic lithosphere that begins to subduct at the specified ages: 30, 60, 100 Ma. Solid lines are the final temperature profiles after 150 Ma of heating. Peak internal temperature anomalies of up to 200°C are consistent with a slab subducted at the Pacific-Gondwanaland margin and heated diffusively for more than 100 Ma.

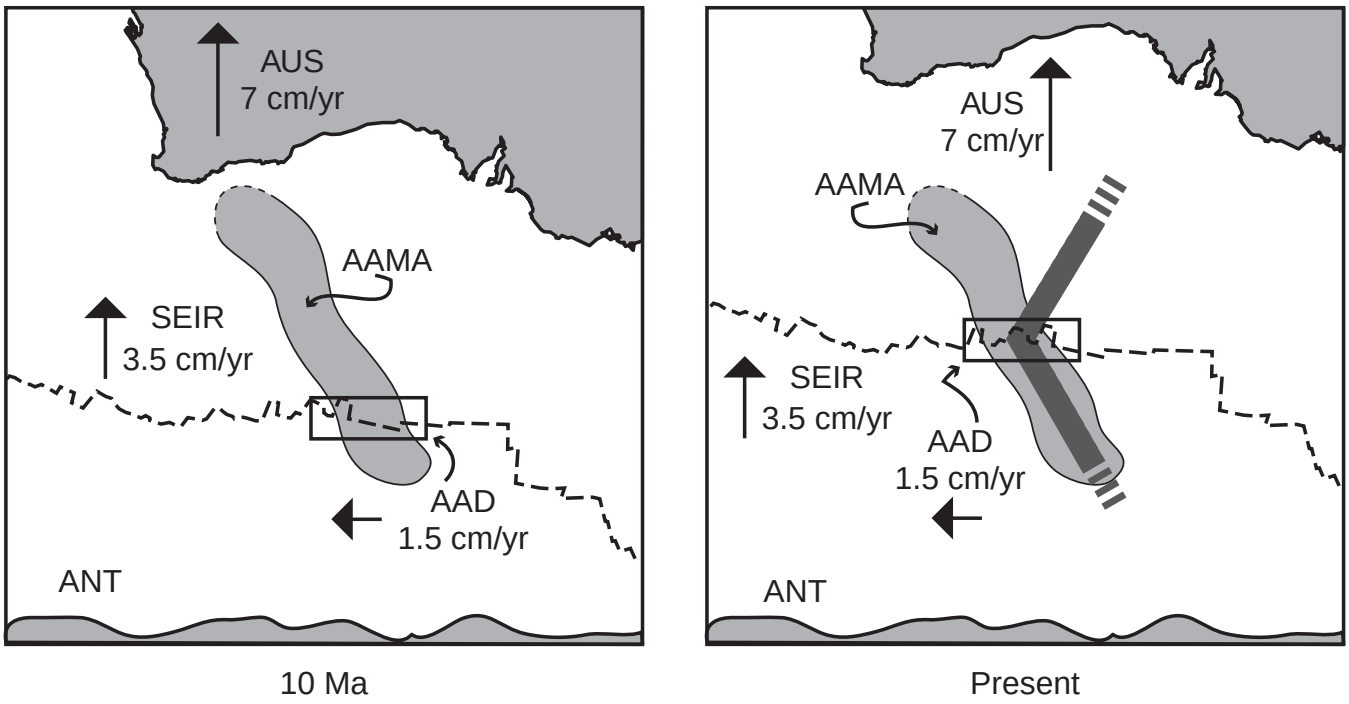

Figure 13. Plate kinematic explanation of the observed westward migration of the AAD and the V-shaped topographic anomaly in the SE Indian Ocean. Assuming that the AAD lies at the intersection of the SEIR and the AAMA, as the SEIR migrates northward at 3.5 cm/y, the AAD will migrate westward at about 1.5 cm/y relative to the ridge. If the topographic anomaly is frozen into the crust, it will form a V-shaped feature (shown with thick grey lines) as the AAD moves to the west relative to the SEIR.

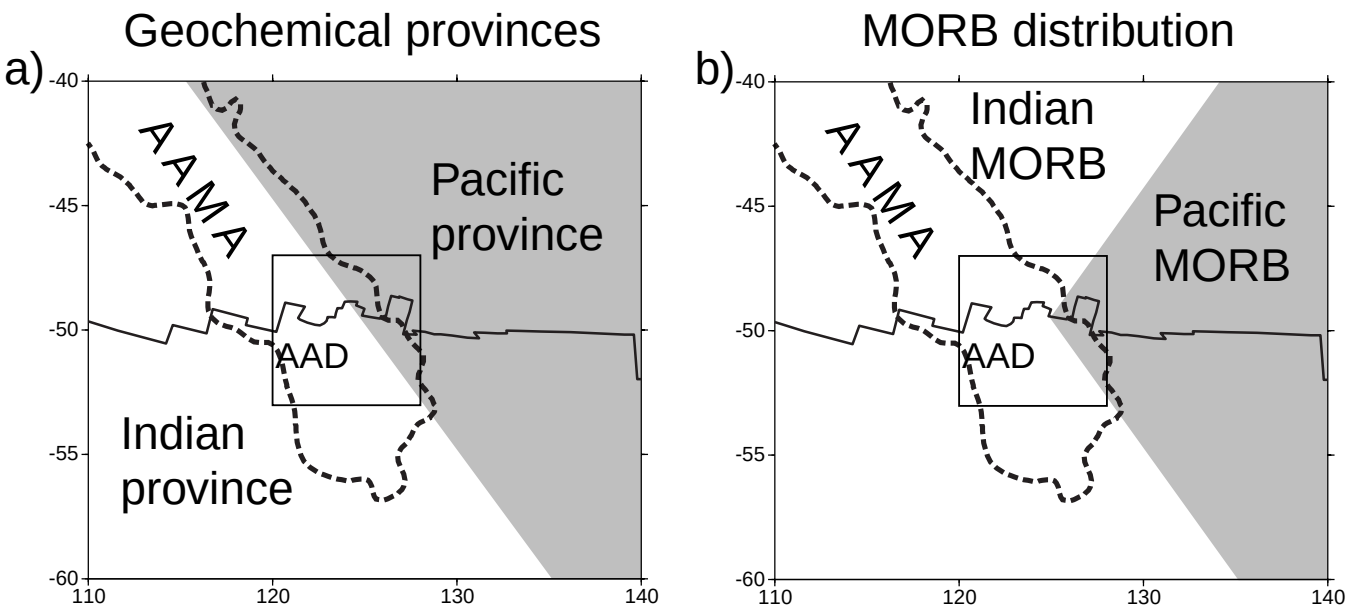

Figure 14. (a) Schematic representation of the AAMA acting as a boundary between Pacific and Indian geochemical provinces in the mantle. The dashed line marks the boundary of the AAMA at 60 km depth. (See Fig. 5a). (b) Potential distribution of MORBs (Indian type, Pacific type) extruded at the surface as the SEIR moves northward and the AAD moves northwestward along the strike of the AAMA. This could be misinterpreted as Pacific asthenosphere penetrating into and displacing Indian asthenosphere along the SEIR.